The Effect of Sn Addition on a Pt/C Electrocatalyst Synthesized by Borohydride Reduction and Hydrothermal Treatment for a Low-Temperature Fuel Cell

Dong-Ha Lim,[a],* Dong-Hyeok Choi,[a] Weon-Doo Lee,[a] Dal-Ryung Park,[b] and Ho-In Lee[a,z]

[a]*School of Chemical and Biological Engineering and Research Center for Energy Conversion and Storage, Seoul National University, Gwanak-gu, Seoul 151-744, Korea*
[b]*Center for Gas Utilization Technology, KOGAS Research and Development Center, Ansan, Kyunggi-do 425-150, Korea*

A 3Pt1Sn/C catalyst was readily synthesized by borohydride reduction and hydrothermal treatment for the anode electrode of a low-temperature fuel cell. The physical and electrochemical characterization of the 3Pt1Sn/C catalyst was performed by transmission electron microscopy (TEM), X-ray diffraction, H_2 adsorption-desorption, methanol oxidation, and CO stripping. In the TEM image, the PtSn nanoparticles were uniformly well-dispersed on the carbon support with an average particle size of around 2.4 nm. The 3Pt1Sn/C catalyst showed higher activity than commercial catalysts, and its onset potential for methanol oxidation was lower, possibly due to the electronic interaction between Pt and Sn and the increase of Pt lattice parameter.
© 2007 The Electrochemical Society. [DOI: 10.1149/1.2710182] All rights reserved.

The most suitable electrocatalyst for a low-temperature fuel cells is Pt metal supported on carbon. However, Pt, which is expensive and whose usage is therefore restrictive, is not the best catalyst for the anode material due to its easy poisoning by the strongly adsorbed CO. It is well known that methanol oxidation on a Pt catalyst produces CO as an intermediate, which is adsorbed on the active sites, resulting in their poisoning.[1] To decrease the amount of Pt and to overcome the problem of CO poisoning, much effort has been made worldwide. One solution is to use secondary metals such as Ru,[2-4] Sn,[5-9] Mo,[10,11] and Cr[12] to enhance the activity for the oxidation of methanol and promote the oxidation of the chemisorbed CO.[13] Among these different possibilities, PtRu alloy is one of the most active catalysts and has been studied by many groups.[2-4,14-16] Ru forms an oxygenated species at lower potentials than Pt, and its presence promotes the oxidation of adsorbed CO to CO_2 through a bifunctional mechanism.[14-16] Recently, PtSn/C catalyst, which has been studied for the oxidation of methanol and ethanol, was used to promote the oxidation of both methanol and CO chemisorbed on the Pt sites.[5,6,17-20] In previous works, PtSn/C catalyst synthesized by an impregnation and modified polyol method showed much higher activity than Pt/C catalyst.[17,21,22] In this study, a 20 wt % 3Pt1Sn/C catalyst was synthesized by borohydride reduction and hydrothermal treatment for use as the anode electrode of a low-temperature fuel cell. The catalyst was characterized using X-ray diffraction (XRD), high-resolution transmission electron microscopy (HRTEM), and cyclic voltammetry.

Experimental

The 20 wt % PtSn/C catalyst with an atomic ratio of Pt/Sn = 3:1 was prepared by borohydride reduction and subsequent hydrothermal treatment. This catalyst was named as 3Pt1Sn/C in this study. The preparation procedure was as follows: 0.022 g of chloroplatinic acid ($H_2PtCl_6 \cdot 6H_2O$, Acros Organics), 0.0032 g of stannous chloride dehydrate ($SnCl_2 \cdot 2H_2O$, Junsei Chemicals), and 0.04 g of pretreated carbon black (Vulcan XC-72R, Cabot Co.) were quantitatively dissolved into 100 mL of distilled water and methanol in a Teflon bottle, and then NaOH was slowly added until the pH reached 11. Under vigorous stirring, 0.01 g of sodium borohydride ($NaBH_4$, Junsei Chemicals) in 50 mL of H_2O was added dropwise to the solution, whereupon the color of the solution immediately turned dark black. The Teflon bottle was held in a stainless steel vessel and sealed tightly. The hydrothermal treatment was performed at 150°C for 3 h in an oven, after which the autoclave was cooled to room temperature and HCl added until the pH was 2. The resultant suspension was filtered, washed with excess amounts of ethanol and distilled water, and dried in a vacuum oven at room temperature overnight. The hydrothermal process employs a high temperature and pressure to bring about the crystallization of PtSn alloy and Sn oxide. The activity of the 3Pt1Sn/C catalyst for methanol oxidation and its electrochemical active surface area (EAS) for H_2 adsorption-desorption were evaluated. XRD, HRTEM, and cyclic voltammetry were employed to characterize the 3Pt1Sn/C catalyst.

The structural characteristics of the synthesized powders were investigated by XRD (Bruker, D8 ADVANCE) analysis using Cu Kα as a radiation source. The working voltage and current were maintained at 40 kV and 30 mA, respectively. The 2θ angular region between 20 and 80° was explored at a scan rate of 1 deg/step. The surface morphology of the PtSn nanoparticles on the surface of carbon black was studied by an HRTEM (JEOL, JEM-3010) operated at 300 kV. The TEM samples were prepared by adding a drop of a suspension, which was made by dispersing the catalyst in ethanol under ultrasonic condition, on a copper grid covered with carbon film, and then evaporating the ethanol.

Electrochemical measurements were carried out in a half-cell using a potentiostat (Gamry Instruments, PC4/750). The catalyst ink was prepared by mixing the catalyst particles with a 5% Nafion solution (DuPont, 1100 EW) and isopropyl alcohol (IPA) under ultrasonic conditions for about 30 min to form a slurry. The ratio of catalyst to Nafion in the catalyst ink was 3:1. A glassy carbon (GC) disk electrode (BAS, MF-2010) with a diameter of 6 mm, which was polished to a mirror finish with a 0.05 μm gamma alumina suspension (Buehler, 40-6301-016) before each experiment, was used as the substrate for the catalyst ink. A drop of catalyst ink was pipetted onto the surface of the GC disk electrode and dried at room temperature. Each electrode was installed into a three-electrode cell with a platinum mesh electrode (Princeton Applied Research, 219810) as the counter electrode and a KCl saturated Ag/AgCl electrode (Bioanalytical System, Inc., MF-2052) as the reference electrode. The reference electrode was located as close as possible to the working electrode. The three-electrode cell was filled with the electrolyte solution and purged with nitrogen gas to remove the dissolved oxygen in the electrolyte solution. In this study, all of the potentials were recorded with respect to a normal hydrogen electrode (NHE).

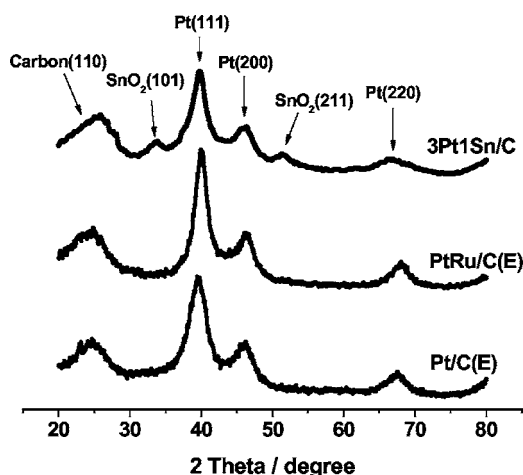* Electrochemical Society Student Member.
z E-mail: hilee@snu.ac.kr

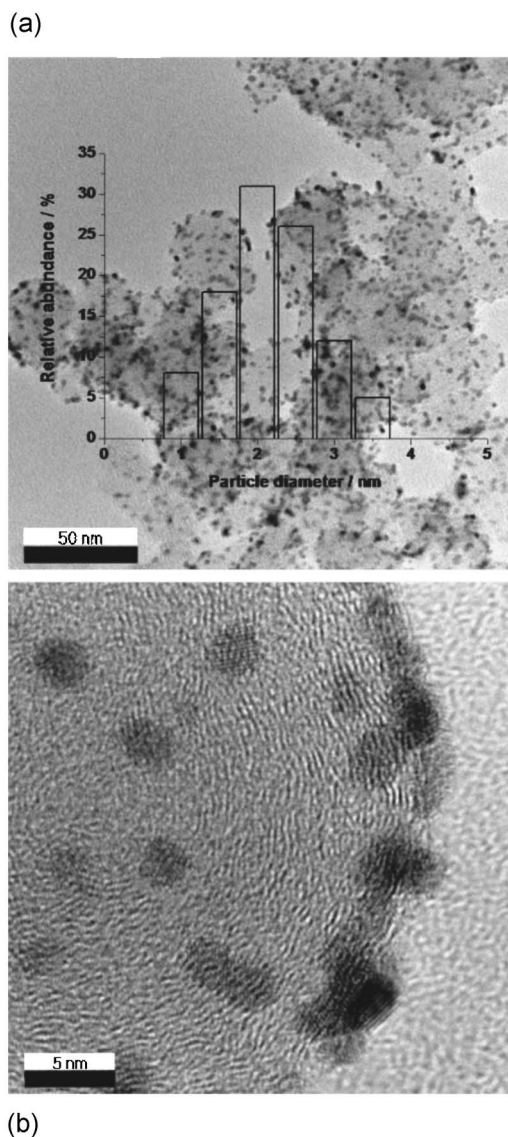**Figure 1.** XRD patterns of the 3Pt1Sn/C, PtRu/C, and Pt/C catalysts.

(a)

(b)

Figure 2. (a) TEM image and (b) HRTEM image of the 3Pt1Sn/C catalyst synthesized by borohydride reduction and hydrothermal treatment.

Results and Discussion

The XRD patterns of the 3Pt1Sn/C catalyst synthesized by borohydride reduction and hydrothermal treatment are shown in Fig. 1. The patterns of the commercial PtRu/C and Pt/C catalysts (E-TEK) are also shown in the same figure for comparison. It is clearly seen from the diffraction pattern of 3Pt1Sn/C in Fig. 1 that both crystalline Pt phase and SnO_2 phase exist. No obvious peaks for Sn are observed in Fig. 1. The Pt (220) peak of the 3Pt1Sn/C shifts slightly to a lower 2θ value compared with that of Pt/C, suggesting the formation of an alloy, which is caused by the interposition of Sn in the face-centered cubic (fcc) structure of Pt. The characterization results are also shown in Table I. The lattice parameter of the commercial PtRu/C catalyst after alloying is smaller than that of the commercial Pt/C catalyst, while the lattice parameter of the 3Pt1Sn/C catalyst is larger than that of the commercial Pt/C catalyst due to lattice expansion after alloying between Pt and Sn. The lattice parameter of the 3Pt1Sn/C catalyst synthesized by borohydride reduction and hydrothermal treatment is similar to that of the bulk 3Pt1Sn solid solution.[19,23] Table I shows that the crystallite size of the 3Pt1Sn/C catalyst is smaller than those of the PtRu/C and Pt/C catalysts. The 3Pt1Sn/C catalyst has a crystallite size of around 2.5 nm, as calculated from the width of the Pt (220) peak according to Scherrer's formula.[24]

In Fig. 2a it can be seen that 3Pt1Sn nanoparticles with a narrow particle size distribution are well-dispersed on the carbon support. The size distribution of 3Pt1Sn nanoparticles on the carbon support was obtained by measuring the sizes of 150 randomly chosen particles from a TEM image. The HR-TEM image of the 3Pt1Sn/C catalyst is shown in Fig. 2b, which shows that the 3Pt1Sn nanoparticles are dispersed on the edges of each grain of the carbon support and are uniform, with an average particle size of around 2.4 nm, which is in good agreement with the XRD data. The good distribution of the 3Pt1Sn nanoparticles is known to be important for the catalytic activity.[20] The 3Pt1Sn nanoparticles deposited on a carbon

support, synthesized by borohydride reduction and hydrothermal treatment, are expected to have good catalytic activity and CO tolerance in the methanol oxidation.

For the measurement of the H_2 adsorption-desorption curve, the potential was cycled between 0 and 1.2 V [vs a normal hydrogen electrode (NHE)] at 20 mV/s in a 0.5 M H_2SO_4 electrolyte solution purged with nitrogen at 25°C. These curves were stabilized after ten cycle in the potential range. Figure 3 shows the H_2 adsorption-desorption curves of the 3Pt1Sn/C, PtRu/C, and Pt/C catalysts. These catalysts exhibit well-defined H_2 adsorption-desorption peaks in the potential region of ca. 0 to 0.25 V (vs NHE) and the adsorption-desorption peaks of oxygen species at around 0.7 V and 1.0 V (vs NHE), which are in a good agreement with the literature values.[25,26] The 3Pt1Sn/C and PtRu/C catalysts show a much less distinct H_2 adsorption-desorption region in comparison with Pt/C, due to the occurrence alloying between Pt and Sn (or Ru).[27,28] The cyclic voltammogram curve of the 3Pt1Sn/C catalyst shows an increase in the current density at the double layer caused by the addition of Sn.[27,28] It can be seen in Fig. 3 that small peaks appear at around 0.53 and 0.75 V, which may be attributed to the adsorption and desorption of oxygen-containing species resulting from the dis-
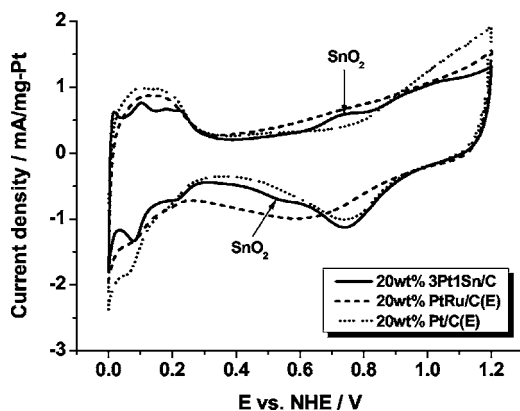
Table I. The physical properties of the 3Pt1Sn/C, commercial PtRu/C, and commercial Pt/C, calculated from the XRD data

Sample	Lattice parameter (nm)	Pt surface area (m²/g)	Crystallite size (nm)
3Pt1Sn/C	0.3963	112	2.5
Pt/C(E)	0.3917	87.4	3.2
PtRu/C(E)	0.3881	77.7	3.6

Figure 3. Cyclic voltammograms of H$_2$ adsorption-desorption on the 3Pt1Sn/C, PtRu/C, and Pt/C catalysts.

Figure 5. Galvanostatic polarization curves for the 3Pt1Sn/C, PtRu/C, and Pt/C catalysts obtained at 40°C in a mixed solution of 0.5 M H$_2$SO$_4$ and 2 M MeOH.

sociation of water on SnO$_2$.[5,6,29] This may be attributed to the presence of SnO$_2$, as observed in the XRD patterns of Fig. 1, which plays a very important role in methanol oxidation and CO oxidation at low potentials.[30]

In order to check the activity of the catalyst for methanol oxidation, a mixed solution of 2 M CH$_3$OH and 0.5 M H$_2$SO$_4$ purged with nitrogen at 40°C was used as the electrolyte solution. The current values were normalized by both the loading amount and the surface area of Pt metal, considering that methanol adsorption and dehydrogenation occur only on the Pt sites at room temperature.[3,15,31-33] The mass- and area-normalized current densities were obtained as shown in Fig. 4. However, the current densities are generally normalized by the amount of loaded metal due to the economic efficiency. In Fig. 4, the mass- and area-normalized cur-
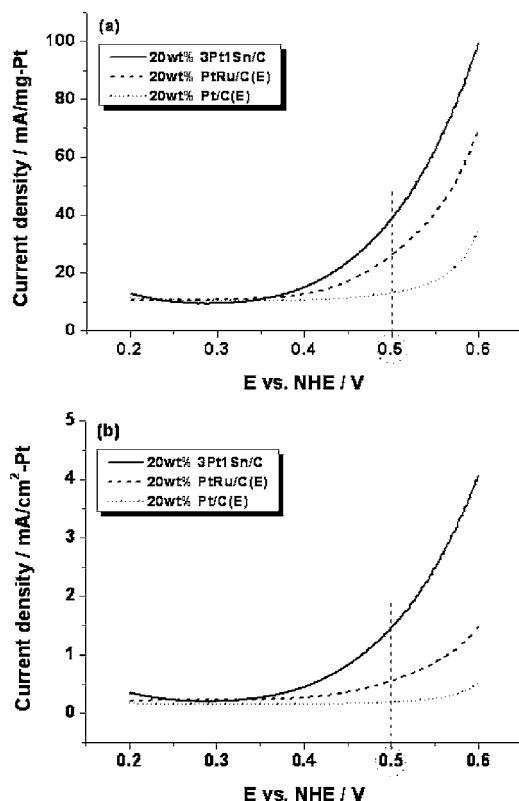

Figure 4. (a) Mass- and (b) area-normalized cyclic voltammograms of MeOH oxidation on the 3Pt1Sn/C, PtRu/C, and Pt/C catalysts.
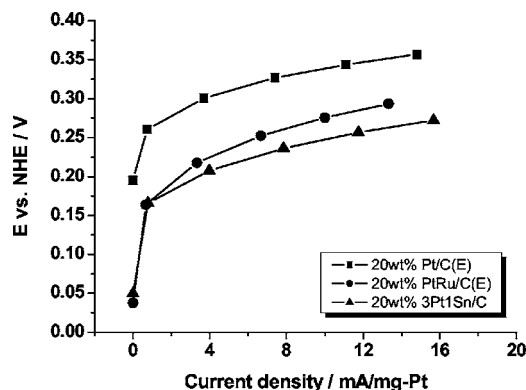
rent densities of methanol oxidation on the 3Pt1Sn/C, PtRu/C, and Pt/C catalysts are shown. The 3Pt1Sn/C catalyst shows higher catalytic activity than the PtRu/C and Pt/C catalysts in both the cases. The current densities of methanol oxidation on the 3Pt1Sn/C and PtRu/C catalysts sharply increase in the region of 0.4–0.5 V (vs NHE), while that on the Pt/C catalyst slightly increases until 0.55 V (vs NHE). The area-normalized current densities were obtained by dividing the measured currents by the calculated electrochemical surface areas from the CO$_{ad}$ stripping test. The area-normalized current density represents the intrinsic activity of the active sites in the electrocatalysts. Because the mass-normalized current density represents the economic efficiency of the catalysts, however, it is generally adopted instead of the area-normalized one in case of similar catalytic environments resulting in the same qualitative trends. The 3Pt1Sn/C catalyst showed a same trend in order being compared with the PtRu/C and Pt/C catalysts between mass- and area-normalized current densities at 0.5 V (vs NHE), as shown in Fig. 4. The difference in gaps of the two defined current densities is due to the different metal dispersions.

According to the results shown in Fig. 4a, the onset potentials of methanol oxidation on the 3Pt1Sn/C, PtRu/C, and Pt/C catalysts are 0.32, 0.35, and 0.45 V, respectively. The onset potential of methanol oxidation is lower on the 3Pt1Sn/C catalyst than on the PtRu/C and Pt/C catalysts.[5,6,17] This indicates that the energy required for methanol oxidation on the 3Pt1Sn/C catalyst is lower, which may be attributed to both the electronic interaction between Pt and Sn and the changes in the Pt lattice parameter due to the addition of Sn.[30,34] The presence of alloyed Sn which expands the lattice allows methanol to adsorb and dissociate, thus allowing the C–H bonds to be broken at lower potentials than that observed on the PtRu/C and Pt/C catalysts.[17] Therefore, the 3Pt1Sn/C catalyst is thought to be a more suitable catalyst for methanol oxidation than the PtRu/C and Pt/C catalysts.

The galvanostatic polarization curves were obtained for the 3Pt1Sn/C, PtRu/C, and Pt/C catalysts at 40°C in a mixed solution of 0.5 M H$_2$SO$_4$ and 2 M MeOH. The current is plotted at mA/mgPt in Fig. 5 to ensure that the data are comparable. It can be seen from Fig. 5 that the 3Pt1Sn/C catalyst shows the best performance over the entire range of polarization. This result is consistent with the result of methanol oxidation presented in Fig. 4.

The activity of the 3Pt1Sn/C catalyst for CO oxidation was investigated by CO stripping voltammetry at 50 mV/s, during which CO was adsorbed on the catalysts at 0.1 V (vs NHE) for 30 min. The CO stripping voltammograms of the 3Pt1Sn/C, PtRu/C, and Pt/C catalysts are shown in Fig. 6. The onset potential of CO oxidation occurs at 0.39 V (vs NHE) for the PtRu/C catalyst and 0.71 V (vs NHE) for the Pt/C catalyst, whereas on the 3Pt1Sn/C catalyst, the onset potential of CO oxidation starts at 0.23 V (vs
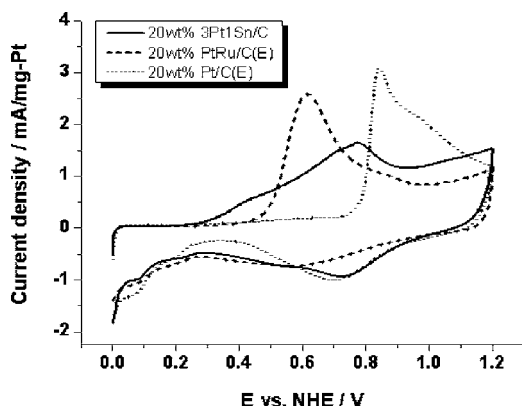
Figure 6. CO stripping voltammograms for the 3Pt1Sn/C, PtRu/C, and Pt/C catalysts obtained at room temperature with a scan rate of 50 mV/s in a 0.5 M H_2SO_4 solution.

NHE), showing a maximum peak at 0.76 V (vs NHE). This indicates that the activity of the 3Pt1Sn/C catalyst for CO oxidation is superior to those of the PtRu/C and Pt/C catalysts. It appears that Sn has the ability to promote the oxidation of adsorbed CO at low potentials.[18] The shift of the onset potential on the 3Pt1Sn/C catalyst may be attributed to the presence of oxygenated species on the Sn sites at a lower potential as compared to the PtRu/C and Pt/C catalysts.[18-20] The superior activity of the 3Pt1Sn/C catalyst can be explained by a bifunctional mechanism. OH adsorbed and formed by the dissociative adsorption of water onto the Sn or Sn oxide sites could oxidize the CO adsorbed onto Pt to CO_2 at lower potentials.[5,6] The shift of the onset potential to a lower value in the CO stripping voltammetry for the PtSn/C catalyst is in agreement with the findings previous works.[5,6,17-20] Vigier et al. reported that SnO_2 could supply oxygen species for the oxidation of CO adsorbed on the adjacent Pt sites, thereby enhancing the oxidation of ethanol at low potentials.[35] Moreover, the range of potentials allowing for the oxidation of CO on the 3Pt1Sn/C catalyst is wider than those on the PtRu/C and Pt/C catalysts. According to Massong et al.,[36] this is due to the presence of adsorbed, linearly bonded CO and bridge-bonded CO on the Pt sites. They claimed that the bridge-bonded CO could be oxidized at a lower potential on PtSn/C than on Pt/C. Therefore, the addition of Sn is thought to prevent CO from poisoning the active Pt sites through the easier oxidation of adsorbed CO.

Conclusions

In conclusion, a 20 wt % 3Pt1Sn/C electrocatalyst was easily synthesized by borohydride reduction and hydrothermal treatment for use as the anode electrode of a low-temperature fuel cell. From both the XRD and HR-TEM results, it was found that the 3Pt1Sn/C nanoparticles were uniformly well dispersed on the carbon support with an average particle size of 2.4 nm. The good distribution of the 3Pt1Sn nanoparticles is known to be an important factor in the catalytic activity. The 3Pt1Sn/C catalyst showed higher catalytic activity for methanol oxidation than the commercial catalysts. The catalytic activity for methanol oxidation was consistent with the galvanostatic polarization curves. The onset potential for methanol oxidation with the 3Pt1Sn/C catalyst was lower, which may be attributed to both the electronic interaction between Pt and Sn and the changes in the Pt lattice parameter due to the addition of Sn. The oxidation of CO on the 3Pt1Sn/C catalyst occurred at a lower potential than that on the commercial catalysts. It appeared that Sn has the ability to pro-

mote the oxidation of adsorbed CO at low potentials. The removal of the CO adsorbed onto Pt proceeded via its reaction with OH adsorbed onto the Sn or Sn oxide sites formed by the dissociative adsorption of water.

References

1. T. Iwasita, H. Hoster, A. John-Anaker, W. F. Lin, and W. Vielstich, *Langmuir*, **16**, 522 (2000).
2. J.-H. Choi, K.-W. Park, B.-K. Kwon, and Y.-E. Sung, *J. Electrochem. Soc.*, **150**, A973 (2003).
3. H. A. Gasteiger, N. Markovic, P. N. Ross, and E. J. Cairns, *J. Electrochem. Soc.*, **141**, 1795 (1994).
4. S.-A. Lee, K.-W. Park, B.-K. Kwon, and Y.-E. Sung, *J. Ind. Eng. Chem. (Seoul, Repub. Korea)*, **9**, 63 (2002).
5. M. Arenz, V. Stamenkovic, B. B. Blizanac, K. J. Mayrhofer, N. M. Markkovic, and P. N. Ross, *J. Catal.*, **232**, 402 (2005).
6. I. Honma and T. Toda, *J. Electrochem. Soc.*, **150**, A1689 (2003).
7. W. S. Cardoso, M. S. P. Francisco, A. M. S. Lucho, and Y. Gushiken, *Solid State Ionics*, **167**, 165 (2004).
8. M. Gotz and H. Wendt, in *Proton Conducting Membrane Fuel Cells II*, S. Gottesfeld and T. F. Fuller, Editors, PV 98-27, p. 291, The Electrochemical Society Proceedings Series, Pennington, NJ (1999).
9. E. Peled, T. Duvdevani, A. Ahron, and A. Melman, *Electrochem. Solid-State Lett.*, **4**, A38 (2001).
10. M. Götz and H. Wendt, *Electrochim. Acta*, **43**, 3637 (1998).
11. A. O. Neto, M. J. Giz, J. Perez, E. A. Ticianelli, and E. R. Gonzalez, *J. Electrochem. Soc.*, **149**, A272 (2002).
12. J.-S. Choi, W.-S. Chung, H.-Y. Ha, T.-H. Lim, I.-H. Oh, S.-A. Hong, and H.-I. Lee, *J. Power Sources*, **156**, 466 (2006).
13. S. Ball, A. Hodgkinson, G. Hoogers, S. Maniguet, D. Thompsett, and B. Wong, *Electrochem. Solid-State Lett.*, **5**, A31 (2002).
14. W. Xu, T. Lu, C. Liu, and W. Xing, *J. Phys. Chem.*, **109**, 14325 (2005).
15. H. A. Gasteiger, N. M. Markovic, and P. N. Ross, Jr., *J. Phys. Chem.*, **99**, 8290 (1995).
16. K.-W. Park and Y.-E. Sung, *J. Ind. Eng. Chem. (Seoul, Repub. Korea)*, **12**, 165 (2006).
17. W. J. Zhou, B. Zhou, W. Z. Li, Z. H. Zhou, S. Q. Song, G. Q. Sun, Q. Xin, S. Douvartzides, M. Goula, and P. Tsiakaras, *J. Power Sources*, **126**, 16 (2004).
18. E. M. Crabb, R. Marshall, and D. Thompsett, *J. Electrochem. Soc.*, **147**, 4440 (2000).
19. F. Colmati, E. Antolini, and E. R. Gonzalez, *Electrochim. Acta*, **50**, 5496 (2005).
20. D.-Y. Lee, S.-W. Hwang, and I.-S. Lee, *J. Power Sources*, **145**, 147 (2005).
21. L. Jiang, G. Sun, S. Sun, J. Liu, S. Tang, H. Li, B. Zhou, and Q. Xin, *Electrochim. Acta*, **50**, 5384 (2005).
22. C. Lamy, S. Rousseau, E. M. Belgasir, C. Coutanceau, and J.-M. Leger, *Electrochim. Acta*, **49**, 3901 (2004).
23. M. Hoheisel, S. Speller, J. Kuntze, A. Atrei, U. Bardi, and W. Heiland, *Phys. Rev. B*, **63**, 245403 (2001).
24. V. Radmiloviae, H. A. Gasteiger, and P. N. Ross, Jr., *J. Catal.*, **154**, 98 (1995).
25. J. R. C. Salgado, E. Antolini, and E. R. Gonzalez, *J. Power Sources*, **138**, 56 (2004).
26. N. M. Markovic, H. A. Gasteiger, P. N. Ross, Jr., X. Jiang, I. Villegas, and M. J. Weaver, *Electrochim. Acta*, **40**, 91 (1995).
27. R. B. Lima, V. Paganin, T. Iwasita, and W. Vielstich, *Electrochim. Acta*, **49**, 85 (2003).
28. E. V. Spinace, A. O. Neto, and M. Linardi, *J. Power Sources*, **129**, 121 (2004).
29. T. Frelink, W. Visscher, and J. A. R. van Veen, *Electrochim. Acta*, **39**, 1871 (1994).
30. S. Mukerjee and J. McBreen, *J. Electrochem. Soc.*, **146**, 600 (1999).
31. M. Christov and K. Sundmacher, *Surf. Sci.*, **1**, 547 (2003).
32. L. Dubau, F. Hahn, C. Countaceau, J.-M. Leger, and C. Lamy, *J. Electroanal. Chem.*, **407**, 554 (2003).
33. Y. Takasu, T. Fujiwara, Y. Murakami, K. Sasaki, M. Oguri, T. Asaki, and W. Sugimoto, *J. Electrochem. Soc.*, **147**, 4421 (2000).
34. A. O. Neto, T. R. R. Vasconcelos, R. W. R. V. Da Silva, M. Linardi, and E. V. Spinace, *J. Appl. Electrochem.*, **35**, 193 (2005).
35. F. Vigier, C. Coutanceau, F. Hahn, E. M. Belgsir, and C. Lamy, *J. Electroanal. Chem.*, **563**, 81 (2004).
36. H. Massong, H. Wang, G. Samjeske, and H. Baltruschat, *Electrochim. Acta*, **46**, 701 (2000).